The Interplay of Structure and Dynamics in the Raman Spectrum of Liquid Water over the Full Frequency and Temperature Range

Tobias Morawietz,[a] Ondrej Marsalek,[b] Shannon R. Pattenaude,[c] Louis M. Streacker,[c] Dor Ben-Amotz,[c] and Thomas E. Markland[a,*]

a) Department of Chemistry, Stanford University, Stanford, CA 94305, United States

b) Faculty of Mathematics and Physics, Charles University, Ke Karlovu 3, 121 16 Prague 2, Czech Republic

c) Department of Chemistry, Purdue University, West Lafayette, IN 47907, United States

*Email: tmarkland@stanford.edu

Abstract

While many Vibrational Raman spectroscopy studies of liquid water have investigated the temperature dependence of the high-frequency O-H stretching region, few have analyzed the changes in the Raman spectrum as a function of temperature over the entire spectral range. Here, we obtain the Raman spectra of water from its melting to boiling point, both experimentally and from simulations using an ab initio-trained machine learning potential. We use these to assign the Raman bands and show that the entire spectrum can be well described as a combination of two temperature-independent spectra. We then assess which spectral regions exhibit strong dependence on the local tetrahedral order in the liquid. Further, this work demonstrates that changes in this structural parameter can be used to elucidate the temperature dependence of the Raman spectrum of liquid water and provides a guide to the Raman features that signal water ordering in more complex aqueous systems.

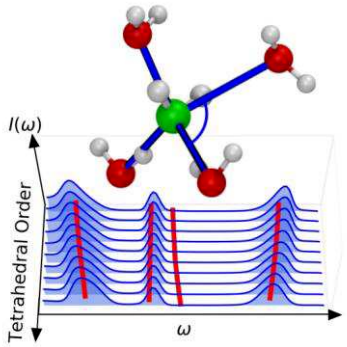

TOC image

Despite the importance of liquid water and the structural and dynamic sensitivity of vibrational Raman spectroscopy,[1] quantitatively linking water spectra and structure remains a challenge for experiment and theory. Indeed, few experimental studies have spanned the entire liquid temperature and vibrational frequency range: from the low frequency intramolecular hydrogen bond (H-bond) stretch, O-H…O at ~180 cm^{-1}, to the high-frequency O-H stretch region at ~3400 cm^{-1}.[2–9] The need for such experimental results is particularly timely as it is becoming increasingly practical to simulate the Raman spectra of water using first principles approaches across the entire frequency range,[10–12] thus providing a strenuous test of these methods' ability to correctly capture and elucidate the structure and dynamics of water. Here we employ a combined experimental and theoretical strategy to address the open questions regarding the origin of vibrational features in the Raman spectra of liquid water from its melting to boiling point.

Many previous experimental Raman[2,8,9,13–16] and Infrared (IR)[16–20] studies have concentrated on analyzing the temperature dependence of the O-H stretching region where an isosbestic point, a region in the spectrum where the intensity is approximately constant upon a change in temperature,[14] is observed. The bimodal profile of the isotropic line shape together with the observation of an isosbestic point has been frequently attributed to an equilibrium between O-H bonds that correspond to water molecules in two different local environments.[9,13,15,21] Although such isosbestic behavior is expected for spectra composed of two components, it can also arise from a continuous distribution of thermally equilibrated structures.[22,23] Theoretical studies have thus sought to simulate and decompose the Raman spectra. For example the temperature dependence of the isotropic Raman O-H stretching band has been shown to be remarkably well reproduced by simulations employing rigid water models using mappings between the vibrational frequency and the local electric field[24–28] while some

early studies have calculated the low frequency terahertz region from time-correlation functions of the polarizability tensor.[29–31] However, more recently it has become possible to use high-level ab initio-based potential energy surfaces[11] or ab initio molecular dynamics (AIMD) calculations with classical[10,12] and even quantum nuclei[12] to make fully first principles predictions of the Raman spectrum at ambient conditions across the entire frequency range.

Here we present a combined experimental and theoretical study of the temperature-dependent Raman spectra of liquid water from its freezing to boiling point over the full frequency range, from ~100 cm^{-1} to ~4200 cm^{-1}. By doing this we address open questions regarding the origin of vibrational features that are more prominent in the Raman than IR spectra and the correlation between the vibrational and structural properties of water. To increase the efficiency of our simulations we employ neural network potentials (NNPs)[32–35] trained to density functional theory calculations (see Supporting Information (SI), sections 1-3). By experimentally and theoretically probing the entire vibrational frequency range here we provide a rigorous assignment of the low-intensity modes in the vibrational spectra and identify several spectral regions, in addition to the O-H stretching region, that exhibit strong dependence on the local tetrahedral order of the liquid. Our results further reveal that the temperature dependence of both the vibrational spectrum of water and its tetrahedral order distribution can be accurately decomposed into a linear combination of two temperature-independent components. By employing a time-dependent analysis of our simulated spectra, we provide theoretical support for the empirical observation that enhanced tetrahedral order is associated with features appearing across the entire frequency range, from the low-frequency H-bond stretch band to the high-frequency O-H stretch band. This analysis allows us to identify the regions that provide the most sensitive spectral signatures of structural ordering in liquid water, thus offering insights into the

origins of these features. The identification of these features will aid in the analysis of other complex aqueous environments ranging from the hydration-shells of solute molecules to catalytic surfaces and biological interfaces.[36–43]

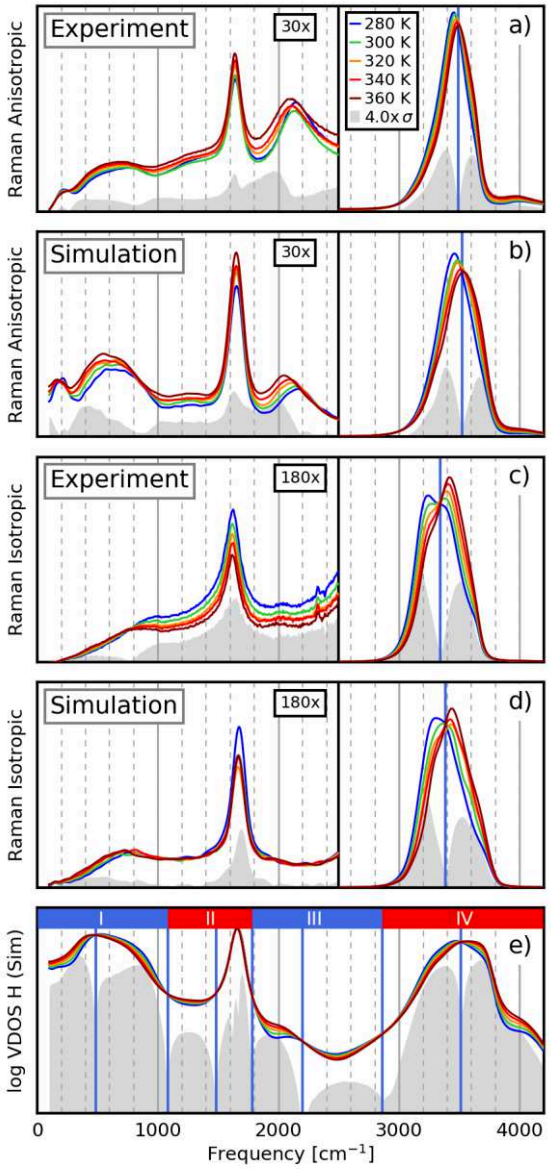

Figure 1. Comparison of the experimental and simulated anisotropic and isotropic reduced Raman spectra (a-d) and the simulated hydrogen vibrational density of states (VDOS, shown on a logarithmic scale to highlight the low-intensity features) (e) of liquid water at different temperatures. For clarity, the low frequency region was scaled by the factor indicated in the plot. All spectra are truncated at 100 cm^{-1} which is the lowest frequency for which accurate

experimental intensities were obtained. All spectra are normalized to unit area. The standard deviation σ, with respect to temperature (shown as grey shading), was used to locate isosbestic points which are depicted as blue lines. The hydrogen VDOS spectrum can be divided into four regions, each of which has an isosbestic point at the center and is separated by isosbestic points from the other regions.

In Figure 1 we compare the experimental (panels a and c) and simulated (panels b and d) anisotropic and isotropic Raman spectra of liquid water. The spectra are presented in a reduced form[44,45] (see SI sections 4-5) that is particularly useful for such a comparison, as it highlights features in the low frequency region, and removes the dependence on the incident laser frequency. Figure 1e shows the temperature-dependent vibrational density of states (VDOS) of the hydrogen atoms (on a logarithmic-scale for better visibility of the low-intensity regions) which exhibits analogous trends to those seen in the Raman spectra. The low-frequency band at ~200 cm^{-1}, which has been attributed to the (intermolecular) H-bond stretching mode,[9] is barely visible in the hydrogen VDOS, but is more prominent in the oxygen VDOS (see SI section 6). The grey shading in Figure 1 shows the standard deviation of the spectral data obtained at different temperatures and thus gives an indication of the temperature sensitivity of different spectral regions. The minima in the standard deviation thus allow for the approximate identification of isosbestic points (frequencies where the spectral intensity is temperature-independent).

The high-frequency O-H stretching region (from ~2500 cm^{-1} to ~4200 cm^{-1}) of the anisotropic and isotropic Raman spectra has been the focus of the majority of previous studies.[2,8,9,13–15,21,24–26,28] As observed in Figure 1a, the anisotropic O-H band consists of a single peak that decreases in intensity and shifts to higher frequencies as the temperature is raised, which resembles the behavior seen in the IR spectrum of liquid water,[46] while the isotropic band has a bimodal profile (Figure 1c). A feature that is not evident in the IR spectrum but appears in

the anisotropic Raman spectrum is the high-frequency band at around 4000 cm^{-1}, which is higher than even the O-H stretch frequency of the isolated molecule (~3750 cm^{-1}). To identify the origin of this feature, which is observed both in our experiments and simulations, we show the synchronous two-dimensional (2D) correlation spectrum[47] of the simulated VDOS in Figure 2a (also see SI section 7). This analysis indicates the frequencies that are positively correlated (red regions) and those that are anticorrelated (blue regions) and thus allows us to identify the vibrational modes with which the high-frequency feature is correlated. As seen in Figure 2b, the 4100 cm^{-1} band is strongly correlated with two bands at lower frequencies – one with its maximum in the libration region (centered at 433 cm^{-1}) and one in the O-H stretch region (centered at 3645 cm^{-1}) – whose sum yields a combined frequency of 4078 cm^{-1}. The fact that this mode is strongly associated with two bands that sum to give its frequency supports an assignment of this feature as a combination band (i.e. arising from anharmonic couplings of two or more fundamental modes at frequencies slightly lower than the sum of the fundamental frequencies). This is in contrast with a previous assignment[48] that, while identifying the 4100 cm^{-1} band as arising from librational-vibrational coupling, assigned it as a combination of a higher frequency librational band (730 cm^{-1}) with the low frequency part of the stretch (3423 cm^{-1}), whereas our simulations suggest it arises from coupling between a higher frequency part of the O-H stretch and a lower frequency librational band.

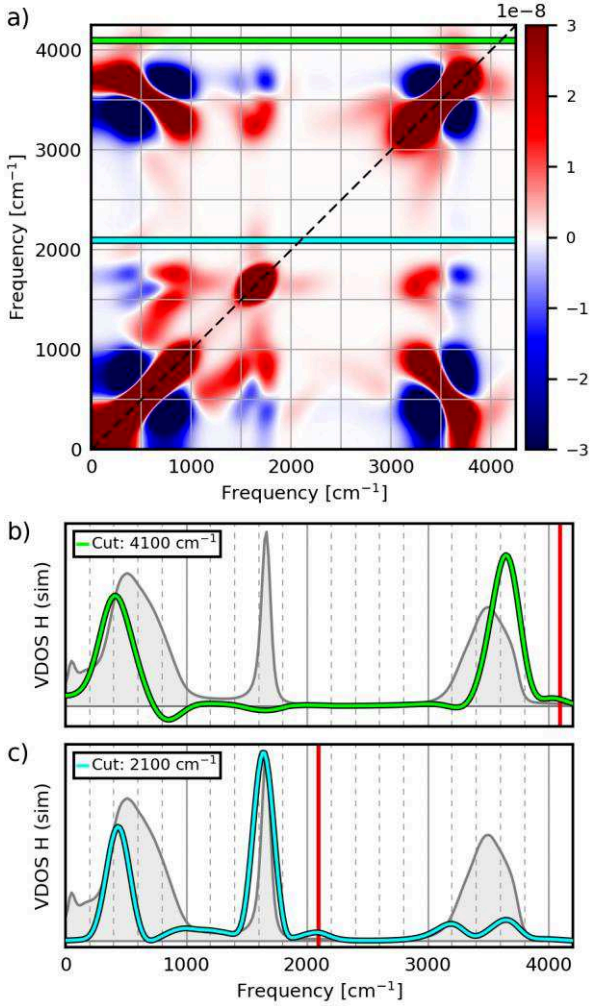

Figure 2. Synchronous two-dimensional correlation spectrum of the simulated hydrogen vibrational density of states (VDOS) at T = 300 K (a). Off-diagonal regions colored in red indicate pairs of frequencies that are positively correlated (intensity of both frequencies in the pair change in the same direction) whereas blue regions indicate an anticorrelation (intensity of both frequencies in the pair change in the opposite direction). Cuts at frequencies of 4100 cm^{-1} and 2100 cm^{-1}, indicated by the light green and light blue horizontal lines in panel (a), are shown in panels (b) and (c). As reference, the full hydrogen VDOS spectrum is shown in grey.

In the low-frequency region of the spectrum, we observe a broad feature centered at ~2100 cm^{-1} (sometimes referred to as the water association band), which is visible in both the experimental and calculated anisotropic Raman spectra. Interestingly, this band at 2100 cm^{-1} was not present in recent anisotropic Raman spectra calculated using the ab initio-based MB-pol model.[11] Experimental and theoretical studies of the IR spectra of liquid water, ice, and

trehalose-water systems have previously assigned this feature to a combination band of the bending mode with a librational mode[49,50] or, alternatively, to the second overtone of a librational mode[51]. Our 2D correlation analysis of our NNP simulations (see Figure 2c) shows that the 2100 cm^{-1} band is a combination band of the low-frequency libration band (centered at 433 cm^{-1}) with the bend vibration (centered at 1631 cm^{-1}) summing to a frequency of 2064 cm^{-1}.

The agreement between our measured and simulated Raman spectra in the O-H stretching region is markedly better than that observed in another recent AIMD simulation, using a different exchange-correlation functional, where the O-H stretching band was red-shifted by ~200 cm^{-1} and significantly broadened compared to the experiment.[10] The location of the isosbestic points in the O-H stretch region are also well reproduced by our simulations (3532 cm^{-1} for the anisotropic spectrum and 3385 cm^{-1} for the isotropic one compared to 3490 cm^{-1} and 3330 cm^{-1} in the experiment). While the overall shape of the simulated anisotropic spectra in the low frequency region deviates slightly from the measured spectra, the position and shape of the individual spectral features and their variation with temperature closely match those seen in the experiment. Having confirmed the agreement between our ab initio-based NNP simulations and the experimental Raman spectra over the full liquid temperature range, we can now use the simulations to relate the observed spectral features to the structural environments in the liquid.

What are the structural changes that lead to the temperature dependence of the different vibrational features occurring across the full frequency range of the Raman spectra? To begin to investigate this question, we first performed a self-modeling curve resolution (SMCR)[52–54] decomposition of the temperature-dependent vibrational spectra obtained from experiment and simulation. SMCR provides a means of decomposing a collection of two or more spectra into a linear combination of different spectral components, each of which has exclusively positive

intensity. For example, SMCR has been used to separate aqueous solution spectra into a linear combination of bulk water and a solute-correlated component to reveal features arising from water molecules that are perturbed by solutes, including ions,[55,56] gases,[57] alcohols,[41,58,59] aromatics,[38,60] surfactants,[61,62] and polymers.[63] Here, we employ an SMCR analysis to assess how accurately the temperature-dependent vibrational spectra can be approximated by a linear combination of two components, whose relative populations, but not spectral shapes, change with temperature.

Figure 3 shows the SMCR decomposition of our experimental and simulated anisotropic Raman spectra as well as the simulated VDOS spectra, which yields a high-temperature "hot" component, closely resembling the full spectrum at 360 K, and a "cold" component, whose intensity increases at low temperatures and whose spectral features are shifted relative to the "hot" component. As shown in SI Figs. S6 and S7, the reconstructed spectra, obtained by combining the two temperature-independent "hot" and "cold" components weighted by their populations, are almost indistinguishable from the original spectra and exhibit integrated fractional errors below 0.01 (see SI section 8) suggesting that the vibrational spectra of water can be accurately represented as a linear combination of two temperature-independent components over its entire liquid temperature range.

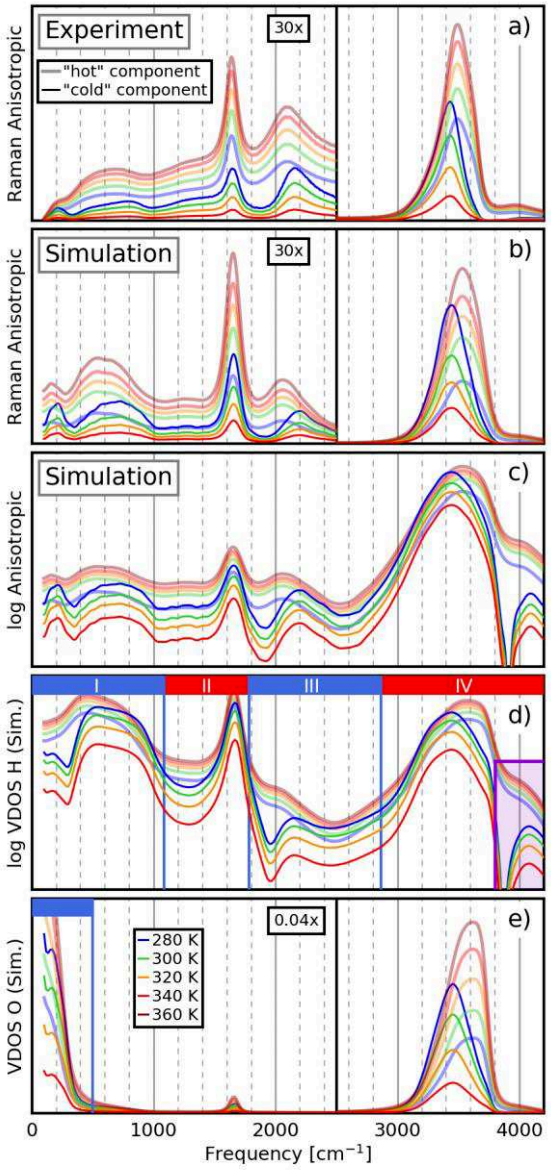

Figure 3. Self-modeling curve resolution (SMCR) decomposition of the experimental and simulated anisotropic Raman spectra (a-c), and the simulated VDOS spectra for the oxygen and hydrogen atoms (d-e). To highlight the close similarities between the anisotropic Raman and the hydrogen VDOS spectra, both are plotted on a logarithmic scale in panels (c) and (d). The four spectral regions in the hydrogen VDOS and an additional low-frequency region in the oxygen VDOS are marked by blue and red bars. The purple area in the hydrogen VDOS (from 3800 cm^{-1} to 4200 cm^{-1}) indicates the region that was selected for the instantaneous frequency analysis of the high-frequency band (shown in Figure 5).

By inspecting the two components we observe that, for the "cold" component, the libration band and the combination band at 2100 cm^{-1} are shifted to higher frequencies, and that a high-frequency peak centered at ~4100 cm^{-1} appears. The most prominent bands in the low temperature SMCR-spectra are peaked near ~200 cm^{-1} and ~3400 cm^{-1} and resemble those observed in ice and solid clathrate hydrates. Specifically, H_2O ice contains prominent bands at ~180 cm^{-1} and ~3100 cm^{-1}.[41,64] Similarly, the Raman spectra of various H_2O clathrate hydrates contain bands peaked near ~210 cm^{-1} and ~3100 cm^{-1}.[65–67] The similar positions of the bands in these tetrahedrally ordered phases to those seen in the SMCR decomposition of the liquid water spectra suggests that these bands may provide spectroscopic probes of the local tetrahedral order in the liquid. We note that even though the band at ~200 cm^{-1} is barely visible in the SMCR decomposed hydrogen VDOS, it can be seen much more prominently in the oxygen VDOS. This behavior is in-line with isotope substitution studies that find larger isotope shifts of this band in the Raman spectrum for a $^{16}O/^{18}O$ substitution compared to a H/D substitution, suggesting that it arises primarily from oxygen motions, consistent with the assignment of this band to the O-H…O H-bond stretch vibration.[45]

Given the good agreement with the experiment, we now use our simulations to assess whether the tetrahedral order in the liquid is indeed the cause of the observed spectral shifts by analyzing the temperature dependence of the local tetrahedral order parameter[68] in its rescaled version[69] (such that it gives a value of 1 for a regular tetrahedron and averages to 0 for an ideal gas, see SI section 3). The local tetrahedral order parameter (or tetrahedrality), q_i, is a measure for the local angular order of water molecule i, based on its four nearest neighbors. The tetrahedrality distribution computed from our simulations (Figure 4a), shows the bimodal structure seen in many previous simulations of liquid water,[43,69,70] with an isosbestic point at $q \approx$

0.67. Upon cooling the distribution shifts to the right, indicating the more predominantly tetrahedral character expected at lower temperatures. To relate the vibrational spectra to the tetrahedrality of the liquid we perform an SMCR decomposition of the tetrahedral order parameter, shown in Figure 4b, analogous to the decomposition of the vibrational spectra. From this we see that, like the spectra, the tetrahedral order distribution can be accurately decomposed into two temperature-independent components. The low-temperature component is shifted to high values of q and the broader high-temperature component is centered at lower q values. While these results demonstrate that the vibrational shifts and the tetrahedrality of the liquid exhibit similar temperature dependence, they alone do not provide direct proof that the spectral shifts are caused by the tetrahedrality of the environment.

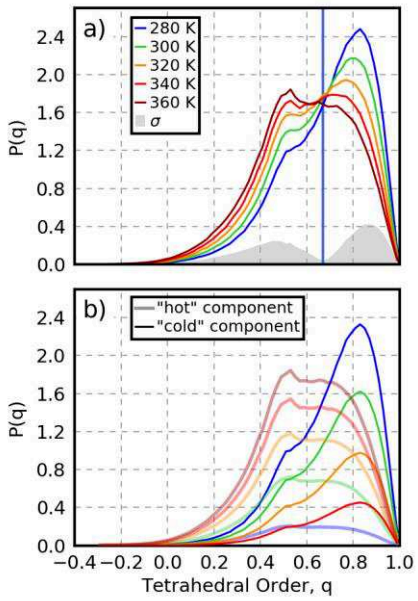

Figure 4. (a) Distribution of the tetrahedral order parameter, q, obtained from ab initio-based simulations of liquid water as function of temperature. An isosbestic point at $q \approx 0.67$ can be identified (shown as blue line). (b) Self-modeling curve resolution (SMCR) decomposition of the tetrahedral order parameter distribution.

To establish the explicit connection between the spectral contribution of a water molecule in the liquid and its tetrahedral order we thus performed a time-dependent analysis of our simulated spectra.[12,71] These results are shown in Figure 5, where the contribution of a given molecule to the vibrational spectrum at a specific point in time is correlated with the instantaneous tetrahedrality of the local hydrogen environment of the same water molecule. For this analysis we employ the VDOS to extract the vibrational motions of individual atoms. The top panels in Figure 5 show results obtained from the VDOS spectra at 320 K, binned as a function of the tetrahedrality parameter over the full frequency range. The bottom panels show how the average frequency in 6 regions of the spectrum changes with the local tetrahedral order of the water molecule. Four of these spectral regions were defined using the seven isosbestic points, identified from the temperature-dependent VDOS (regions I – IV, defined in Figure 1e). The other two were chosen to be the 4000 cm^{-1} combination band identified earlier (defined in Figure 3d) and the 200 cm^{-1} O-H…O H-bond stretch vibration in the oxygen VDOS (Figure 3e).

The results in Figure 5 (bottom panels) demonstrate that there is a direct correlation between vibrational frequency and tetrahedrality in all spectral regions: in some regions the spectrum shifts to higher frequencies as the tetrahedrality increases while in others it shifts to lower frequencies. The O-H stretching band (region IV) is inversely correlated with the tetrahedral order, while the low frequency H-bond stretching band (oxygen VDOS), the libration band (region I), the combination band at 2100 cm^{-1} (region III), and the high-frequency combination band near 4000 cm^{-1}, all are positively correlated. We observe that the bend (region II) displays the least sensitivity with regards to tetrahedral order. The direction of all spectral shifts with tetrahedrality is consistent with the locations of these features in the SMCR component spectra. For instance, in the O-H stretching region the “cold” component, which is

associated with high tetrahedrality, is shifted to lower frequencies, which follows the trend seen in the correlation plot (Figure 5, lower panel, region IV) where a shift to lower frequency values is observed as the tetrahedrality increases.

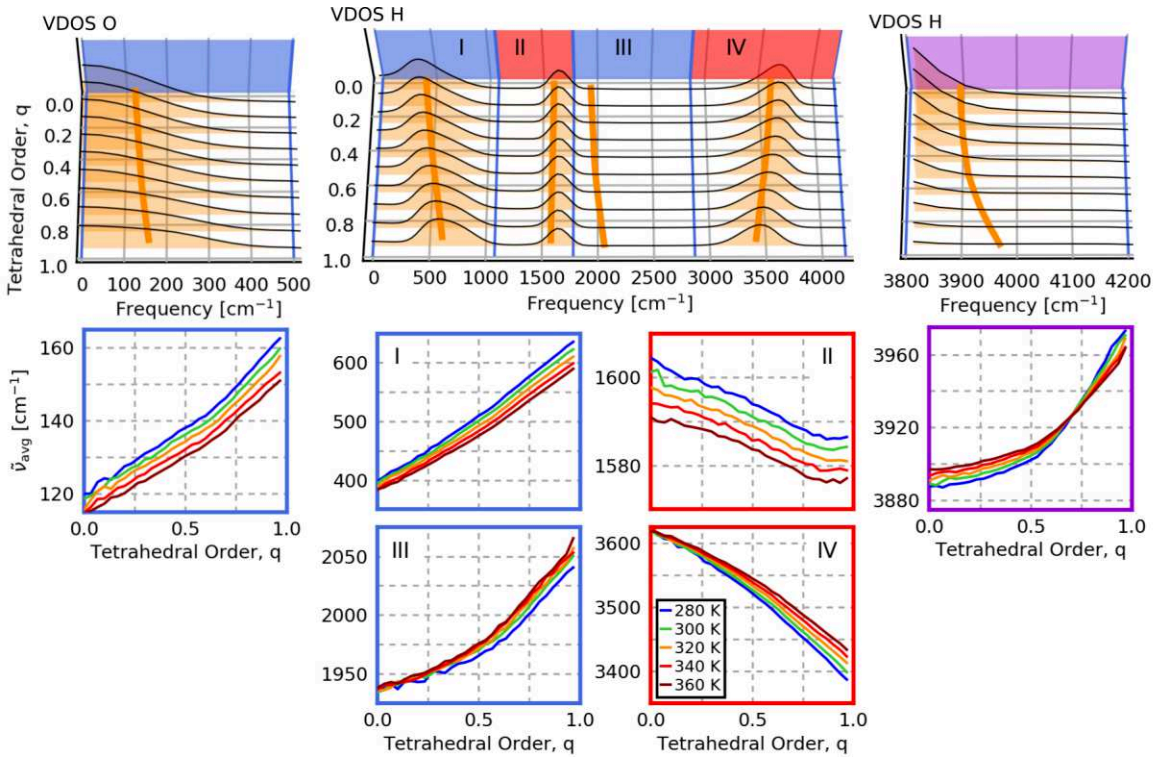

Figure 5. Instantaneous frequency analysis of the simulated hydrogen and oxygen VDOS spectra as function of the tetrahedral order parameter, *q*. The top panels show the VDOS spectrum at a single temperature (T = 320 K), decomposed into contributions from molecules with a given tetrahedral order in the liquid water simulation. The orange lines indicate the average value of the spectrum within the specified region. The bottom panels show the correlation of the average peak values with q for the six different regions and all temperatures.

The similarity of the curves pertaining to different temperature shown in the lower panels of Figure 5 further reveal that the correlation of the average peak frequency with the tetrahedrality is relatively insensitive to temperature. This implies that the correlation between tetrahedrality (*q*) and spectral frequency observed at a single temperature is sufficient to approximately reconstruct the average peak positions at any temperature, given the *q* distribution

at that temperature. This frequency-structure correlation analysis, combined with the other results presented above, provide compelling evidence that the temperature dependence of the Raman spectrum of water is in fact largely correlated to a single structural parameter: the tetrahedrality of the liquid.

In summary, we have presented experiments and simulations of the temperature- and polarization-dependent Raman spectra of liquid water over the entire vibrational frequency range. We have shown that ab initio simulations, accelerated by machine learning potentials, are able to accurately capture subtle temperature-dependent changes in the Raman spectrum of water and employed a 2D correlation analysis of the simulated spectra to assign the Raman bands. Subsequently, by linking the vibrational motions of water to the time-dependent structural features, we have demonstrated that a single structural parameter, the local tetrahedrality, is sufficient to predict the temperature dependence of the vibrational spectrum of liquid water across the whole frequency range. This analysis has enabled us to identify several spectral regions that are strongly correlated with tetrahedral order and thus could be employed in future studies to probe the structural order of water molecules surrounding various solutes and confined within more complex environments.

Acknowledgements

This material is based upon work supported by the National Science Foundation under Grant No. CHE-1652960 to T.E.M. and Grant No. CHE-1464904 to D.B.A. T.E.M. also acknowledges support from a Cottrell Scholarship from the Research Corporation for Science Advancement and the Camille Dreyfus Teacher-Scholar Awards Program. T.M. is grateful for financial support by the DFG (MO 3177/1-1). We thank Andrés Montoya-Castillo for useful discussions and

Aaron Urbas of the Bioassay Methods Group at the National Institute of Standards and Technology for allowing us to borrow the NIST SRM® 2243 used for this study.

Supporting Information. Neural network parametrization; details of the density functional theory calculations; simulation details; discussion on the prefactor for the experimental and simulated Raman spectra; temperature-dependent hydrogen and oxygen VDOS; time-dependent VDOS and two-dimensional frequency analysis; accuracy of the SMCR decomposition

References

(1) Bakker, H. J.; Skinner, J. L. Vibrational Spectroscopy as a Probe of Structure and Dynamics in Liquid Water. *Chem. Rev.* **2010**, *110*, 1498–1517.

(2) Scherer, J. R.; Go, M. K.; Kint, S. Raman Spectra and Structure of Water from -10 to 90°. *J. Phys. Chem.* **1974**, *78*, 1304–1313.

(3) Zhelyaskov, V.; Georgiev, G.; Nickolov, Z.; Miteva, M. Concentration (D2O in H2O) and Temperature Raman Study of the Molecular Interactions in the OD Stretching Spectra of D2O and D2O/H2O Mixtures Using the Fourier Deconvolution Technique. *J. Raman Spectrosc.* **1989**, *20*, 67–75.

(4) Bray, A.; Chapman, R.; Plakhotnik, T. Accurate Measurements of the Raman Scattering Coefficient and the Depolarization Ratio in Liquid Water. *Appl. Opt.* **2013**, *52*, 2503–2510.

(5) De Santis, A.; Frattini, R.; Sampoli, M.; Mazzacurati, V.; Nardone, M.; Ricci, M. A.; Ruocco, G. Raman Spectra of Water in the Translational and Librational Regions: I. Study of the Depolarization Ratio. *Mol. Phys.* **1987**, *61*, 1199–1212.

(6) Walrafen, G. E. Spontaneous and Stimulated Raman Spectra from Water and Aqueous

Solutions. In *Structure of Water and Aqueous Solutions*; Luck, W. A. P., Ed.; Verlag Chemie: Weinheim, 1974; pp 301–321.

(7) Murphy, W. F.; Bernstein, H. J. Raman Spectra and an Assignment of the Vibrational Stretching Region of Water. *J. Phys. Chem.* **1972**, *76*, 1147–1152.

(8) Hare, D. E.; Sorensen, C. M. Raman Spectroscopic Study of Bulk Water Supercooled to -33 °C. *J. Chem. Phys.* **1990**, *93* (1), 25–33.

(9) Walrafen, G. E.; Fisher, M. R.; Hokmabadi, M. S.; Yang, W. -H. Temperature Dependence of the Low- and High-frequency Raman Scattering from Liquid Water. *J. Chem. Phys.* **1986**, *85* (12), 6970–6982.

(10) Wan, Q.; Spanu, L.; Galli, G. A.; Gygi, F. Raman Spectra of Liquid Water from Ab Initio Molecular Dynamics: Vibrational Signatures of Charge Fluctuations in the Hydrogen Bond Network. *J. Chem. Theory Comput.* **2013**, *9* (9), 4124–4130.

(11) Medders, G. R.; Paesani, F. Infrared and Raman Spectroscopy of Liquid Water Through "first-Principles" many-Body Molecular Dynamics. *J. Chem. Theory Comput.* **2015**, *11* (3), 1145–1154.

(12) Marsalek, O.; Markland, T. E. Quantum Dynamics and Spectroscopy of Ab Initio Liquid Water: The Interplay of Nuclear and Electronic Quantum Effects. *J. Phys. Chem. Lett.* **2017**, *8* (7), 1545–1551.

(13) D'Arrigo, G.; Maisano, G.; Mallamace, F.; Migliardo, P.; Wanderlingh, F. Raman Scattering and Structure of Normal and Supercooled Water. *J. Chem. Phys.* **1981**, *75* (9), 4264–4270.

(14) Walrafen, G. E.; Hokmabadi, M. S.; Yang, W. -H. Raman Isosbestic Points from Liquid Water. *J. Chem. Phys.* **1986**, *85* (12), 6964–6969.

(15) Sun, Q. Local Statistical Interpretation for Water Structure. *Chem. Phys. Lett.* **2013**, *568–569*, 90–94.

(16) Wang, Z.; Pakoulev, A.; Pang, Y.; Dlott, D. D. Vibrational Substructure in the OH Stretching Band of Water. *Chem. Phys. Lett.* **2003**, *378* (3–4), 281–288.

(17) Woutersen, S.; Emmerichs, U.; Bakker, H. J. Femtosecond Mid-Infrared Pump-Probe Spectroscopy of Liquid Water: Evidence for a Two-Component Structure. *Science (80-.).* **1997**, *278*, 658–660.

(18) Laenen, R.; Rauscher, C.; Laubereau, A. Dynamics of Local Substructures in Water Observed by Ultrafast Infrared Hole Burning. *Phys. Rev. Lett.* **1998**, *80* (12), 2622–2625.

(19) Laenen, R.; Rauscher, C.; Laubereau, A. Local Substructures of Water Studied by Transient Hole-Burning Spectroscopy in the Infrared: Dynamics and Temperature Dependence. *J. Phys. Chem. B* **1998**, *102* (46), 9304–9311.

(20) Tokmakoff, A. Shining Light on the Rapidly Evolving Structure of Water. *Science (80-.).* **2007**, *317*, 54–55.

(21) Harada, Y.; Miyawaki, J.; Niwa, H.; Yamazoe, K.; Pettersson, L. G. M.; Nilsson, A. Probing the OH Stretch in Different Local Environments in Liquid Water. *J. Phys. Chem. Lett.* **2017**, *8* (22), 5487–5491.

(22) Geissler, P. L. Temperature Dependence of Inhomogeneous Broadening: On the Meaning of Isosbestic Points. *J. Am. Chem. Soc.* **2005**, *127* (42), 14930–14935.

(23) Smith, J. D.; Cappa, C. D.; Wilson, K. R.; Cohen, R. C.; Geissler, P. L.; Saykally, R. J. Unified Description of Temperature-Dependent Hydrogen-Bond Rearrangements in Liquid Water. *Proc. Natl. Acad. Sci. U.S.A.* **2005**, *102* (40), 14171–14174.

(24) Corcelli, S. A.; Lawrence, C. P.; Skinner, J. L. Combined Electronic Structure/molecular

Dynamics Approach for Ultrafast Infrared Spectroscopy of Dilute HOD in Liquid H 2O and D 2O. *J. Chem. Phys.* **2004**, *120* (17), 8107–8117.

(25) Corcelli, S. A.; Skinner, J. L. Infrared and Raman Line Shapes of Dilute HOD in Liquid H 2O and D 2O from 10 to 90°C. *J. Phys. Chem. A* **2005**, *109* (28), 6154–6165.

(26) Auer, B. M.; Skinner, J. L. IR and Raman Spectra of Liquid Water: Theory and Interpretation. *J. Chem. Phys.* **2008**, *128*, 224511.

(27) Yang, M.; Skinner, J. L. Signatures of Coherent Vibrational Energy Transfer in IR and Raman Line Shapes for Liquid Water. *Phys. Chem. Chem. Phys.* **2010**, *12* (4), 982–991.

(28) Tainter, C. J.; Ni, Y.; Shi, L.; Skinner, J. L. Hydrogen Bonding and Oh-Stretch Spectroscopy in Water: Hexamer (Cage), Liquid Surface, Liquid, and Ice. *J. Phys. Chem. Lett.* **2013**, *4* (1), 12–17.

(29) Madden, P. A.; Impey, R. W. On the Infrared and Raman Spectra of Water in the Region 5-250 Cm-1. *Chem. Phys. Lett.* **1986**, *123* (6), 502–506.

(30) Mazzacurati, V.; Ricci, M. A.; Ruocco, G.; Sampoli, M. Low-Frequency Raman Spectra of Liquid Water: A Molecular Dynamics Simulation. *Chem. Phys. Lett.* **1989**, *159* (4), 383–387.

(31) Bursulaya, B. D.; Kim, H. J. Spectroscopic and Dielectric Properties of Liquid Water: A Molecular Dynamics Simulation Study. *J. Chem. Phys.* **1998**, *109* (12), 4911–4919.

(32) Behler, J.; Parrinello, M. Generalized Neural-Network Representation of High-Dimensional Potential-Energy Surfaces. *Phys. Rev. Lett.* **2007**, *98* (14), 146401.

(33) Artrith, N.; Urban, A. An Implementation of Artificial Neural-Network Potentials for Atomistic Materials Simulations: Performance for TiO2. *Comput. Mater. Sci.* **2016**, *114*, 135–150.

(34) Behler, J. Perspective: Machine Learning Potentials for Atomistic Simulations. *J. Chem. Phys.* **2016**, *145* (17), 170901.

(35) Morawietz, T.; Singraber, A.; Dellago, C.; Behler, J. How van Der Waals Interactions Determine the Unique Properties of Water. *Proc. Natl. Acad. Sci. U.S.A.* **2016**, *113* (30), 8368–8373.

(36) Heyden, M.; Bründermann, E.; Heugen, U.; Niehues, G.; Leitner, D. M.; Havenith, M. Long-Range Influence of Carbohydrates on the Solvation Dynamics of Water-Answers from Terahertz Absorption Measurements and Molecular Modeling Simulations. *J. Am. Chem. Soc.* **2008**, *130*, 5773–5779.

(37) Artrith, N.; Kolpak, A. M. Understanding the Composition and Activity of Electrocatalytic Nanoalloys in Aqueous Solvents: A Combination of DFT and Accurate Neural Network Potentials. *Nano Lett.* **2014**, *14* (5), 2670–2676.

(38) Gierszal, K. P.; Davis, J. G.; Hands, M. D.; Wilcox, D. S.; Slipchenko, L. V.; Ben-Amotz, D. Π-Hydrogen Bonding in Liquid Water. *J. Phys. Chem. Lett.* **2011**, *2* (22), 2930–2933.

(39) Fayer, M. D.; Levinger, N. E. Analysis of Water in Confined Geometries and at Interfaces. *Annu. Rev. Anal. Chem.* **2010**, *3*, 89–107.

(40) Crans, D. C.; Levinger, N. E. The Conundrum of pH in Water Nanodroplets: Sensing pH in Reverse Micelle Water Pools. *Acc. Chem. Res.* **2012**, *45*, 1637–1645.

(41) Davis, J. G.; Gierszal, K. P.; Wang, P.; Ben-Amotz, D. Water Structural Transformation at Molecular Hydrophobic Interfaces. *Nature* **2012**, *491* (7425), 582–585.

(42) Bakulin, A. A.; Cringus, D.; Pieniazek, P. A.; Skinner, J. L.; Jansen, T. L. C.; Pshenichnikov, M. S. Dynamics of Water Confined in Reversed Micelles: Multidimensional Vibrational Spectroscopy Study. *J. Phys. Chem. B* **2013**, *117*, 15545–

15558.

(43) Russo, D.; Laloni, A.; Filabozzi, A.; Heyden, M. Pressure Effects on Collective Density Fluctuations in Water and Protein Solutions. *Proc. Natl. Acad. Sci. U.S.A.* **2017**, *114*, 11410–11415.

(44) Brooker, M. H.; Nielsen, O. F.; Praestgaard, E. Assessment of Correction Procedures for Reduction of Raman Spectra. *J. Raman Spectrosc.* **1988**, *19* (2), 71–78.

(45) Brooker, M. H.; Hancock, G.; Rice, B. C.; Shapter, J. Raman Frequency and Intensity Studies of Liquid H2O, H218O and D2O. *J. Raman Spectrosc.* **1989**, *20* (10), 683–694.

(46) Maréchal, Y. The Molecular Structure of Liquid Water Delivered by Absorption Spectroscopy in the Whole IR Region Completed with Thermodynamics Data. *J. Mol. Struct.* **2011**, *1004* (1–3), 146–155.

(47) Noda, I. Generalized Two-Dimensional Correlation Method Applicable to Infrared, Raman, and Other Types of Spectroscopy. *Appl. Spectrosc.* **1993**, *47* (9), 1329–1336.

(48) Walrafen, G. E.; Pugh, E. Raman Combinations and Stretching Overtones from Water, Heavy Water, and NaCl in Water at Shifts to Ca. 7000 Cm-1. *J. Solut. Chem.* **2004**, *33* (1), 81–97.

(49) Maréchal, Y. Infrared Spectra of Water. I. Effect of Temperature and of *H* / *D* Isotopic Dilution. *J. Chem. Phys.* **1991**, *95* (8), 5565–5573.

(50) McCoy, A. B. The Role of Electrical Anharmonicity in the Association Band in the Water Spectrum. *J. Phys. Chem. B* **2014**, *118* (28), 8286–8294.

(51) Devlin, J. P.; Sadlej, J.; Buch, V. Infrared Spectra of Large H 2 O Clusters: New Understanding of the Elusive Bending Mode of Ice. *J. Phys. Chem. A* **2001**, *105* (6), 974–983.

(52) Lawton, W. H.; Sylvestre, E. A. Self Modeling Curve Resolution. *Technometrics* **1971**, *13* (3), 617–633.

(53) Tauler, R.; Smilde, A.; Kowalski, B. Selectivity, Local Rank, Three-way Data Analysis and Ambiguity in Multivariate Curve Resolution. *J. Chemom.* **1995**, *9* (1), 31–58.

(54) Jiang, J. H.; Liang, Y.; Ozaki, Y. Principles and Methodologies in Self-Modeling Curve Resolution. *Chemom. Intell. Lab. Syst.* **2004**, *71*, 1–12.

(55) Daly Jr., C. A.; Streacker, L. M.; Sun, Y.; Pattenaude, S. R.; Petersen, P. B.; Corcelli, S. A.; Ben-Amotz, D. Decomposition of the Experimental Raman and Infrared Spectra of Acidic Water into Proton, Special Pair, and Counter-Ion Contributions. *J. Phys. Chem. Lett.* **2017**, *8*, 5246–5252.

(56) Rankin, B. M.; Ben-Amotz, D. Expulsion of Ions from Hydrophobic Hydration Shells. *J. Am. Chem. Soc.* **2013**, *135* (24), 8818–8821.

(57) Zukowski, S. R.; Mitev, P. D.; Hermansson, K.; Ben-Amotz, D. CO 2 Hydration Shell Structure and Transformation. *J. Phys. Chem. Lett.* **2017**, *8* (13), 2971–2975.

(58) Rankin, B. M.; Ben-Amotz, D.; Van Der Post, S. T.; Bakker, H. J. Contacts between Alcohols in Water Are Random rather than Hydrophobic. *J. Phys. Chem. Lett.* **2015**, *6* (4), 688–692.

(59) Mochizuki, K.; Pattenaude, S. R.; Ben-Amotz, D. Influence of Cononsolvency on the Aggregation of Tertiary Butyl Alcohol in Methanol-Water Mixtures. *J. Am. Chem. Soc.* **2016**, *138* (29), 9045–9048.

(60) Scheu, R.; Rankin, B. M.; Chen, Y.; Jena, K. C.; Ben-Amotz, D.; Roke, S. Charge Asymmetry at Aqueous Hydrophobic Interfaces and Hydration Shells. *Angew. Chem.* **2014**, *53* (36), 9560–9563.

(61) Long, J. A.; Rankin, B. M.; Ben-Amotz, D. Micelle Structure and Hydrophobic Hydration. *J. Am. Chem. Soc.* **2015**, *137* (33), 10809–10815.

(62) Pattenaude, S. R.; Rankin, B. M.; Mochizuki, K.; Ben-Amotz, D. Water-Mediated Aggregation of 2-Butoxyethanol. *Phys. Chem. Chem. Phys.* **2016**, *18* (18), 24937–24943.

(63) Mochizuki, K.; Ben-Amotz, D. Hydration-Shell Transformation of Thermosensitive Aqueous Polymers. *J. Phys. Chem. Lett.* **2017**, *8* (7), 1360–1364.

(64) Kanno, H.; Tomikawa, K.; Mishima, O. Raman Spectra of Low- and High-Density Amorphous Ices. *Chem. Phys. Lett.* **1998**, *293* (5–6), 412–416.

(65) Takasu, Y.; Iwai, K.; Nishio, I. Low Frequency Raman Profile of Type II Clathrate Hydrate of THF and Its Application for Phase Identification. *J. Phys. Soc. Jpn.* **2003**, *72* (5), 1287–1291.

(66) Sugahara, K.; Sugahara, T.; Ohgaki, K. Thermodynamic and Roman Spectroscopic Studies of Xe and Kr Hydrates. *J. Chem. Eng. Data* **2005**, *50* (1), 274–277.

(67) Chazallon, B.; Focsa, C.; Charlou, J.-L.; Bourry, C.; Donval, J.-P. A Comparative Raman Spectroscopic Study of Natural Gas Hydrates Collected at Different Geological Sites. *Chem. Geol.* **2007**, *244* (1–2), 175–185.

(68) Chau, P.; Hardwick, A. J. A New Order Parameter for Tetrahedral Configurations. *Mol. Phys.* **1998**, *93* (3), 511–518.

(69) Errington, J.; Debenedetti, P. Relationship between Structural Order and the Anomalies of Liquid Water. *Nature* **2001**, *409* (6818), 318–321.

(70) Paolantoni, M.; Faginas Lago, N.; Alberti, M.; Laganà, A. Tetrahedral Ordering in Water: Raman Profiles and Their Temperature Dependence. *J. Phys. Chem. A* **2009**, *113* (52), 15100–15105.

(71) Napoli, J. A.; Marsalek, O.; Markland, T. E. Decoding the Spectroscopic Features and Timescales of Aqueous Proton Defects. *arXiv:1709.05740* **2017**.